Surface Potential Imaging of Solution Processable Acene-Based Thin Film Transistors**

By *Lucile C. Teague, Behrang H. Hamadani, Oana D. Jurchescu, Sankar Subramanian, John E. Anthony, Thomas N. Jackson, Curt A. Richter, David J. Gundlach,* and *James G. Kushmerick**

Thin-film electronic devices fabricated using organic semiconductors, insulators, and conductors are expected to greatly impact the semiconductor electronics industry by significantly reducing manufacturing costs and expanding the applicability of active thin-film electronics. With that, organic thin-film transistors (OTFTs) have been a topic of intense interest for over a decade.[1–3] Despite significant improvements to the electrical performance of OTFTs over this time, surprisingly little is known about the fundamental mechanisms governing charge injection and transport in the transistor channel. Scanning probe microscopy methods have become the popular tool for studying the intricate details of these systems. Early work utilized conductive-probe atomic force microscopy (AFM) measurements at discrete points within OTFTs to probe potential drops at the device contacts[4] and at grain boundaries[5,6] within the active organic layer.

Following these experiments, several groups have reported the use of scanning Kelvin probe microscopy (SKPM) to characterize charge transport in a range of OTFTs.[7–12] SKPM affords unique insight into device behavior since it provides the spatially resolved surface potential map of an operating device. To date, SKPM studies have focused on the influences of contact resistance on device performance, including comparisons of top- versus bottom-contact devices[7] and the role of source and drain electrode metallurgy.[8,10] Additional SKPM studies have investigated the variation in surface potential at grain boundaries in evaporated organic thin films, similar to those used in OTFTs.[13] Perhaps most importantly, in a number of these earlier experiments it was found that the potential drop at the electrode/organic semiconductor interface can be on the order of several volts, indicating that the electrical performance of the devices in those instances is contact-limited.[4,7,8,10] In this paper, we present an SKPM study of the potential distribution in solution-processed, bottom-contact OTFTs to determine the role of film microstructure on device performance. By examining devices with a series of channel lengths, we are able to correlate the potential profile across the device and the morphology of the organic layer within the channel to the measured device mobility.

Thin-film transistors prepared from spun-cast fluorinated 5,11-bis(triethylsilylethynyl) anthradithiophene (diF-TESADT) on pentafluorobenzene thiol (PFBT)[14] functionalized electrodes (see schematic in Fig. 1) provide an excellent platform to study potential profiles in functioning devices since the unique properties of the system lead to the formation of large ($\approx 10\,\mu m$) grains that nucleate and grow from the electrodes into the channel region.[15,16] Consistent with this grain growth, we typically observe three unique microstructures within the transistor channel: first a highly ordered channel, with large grains bridging the source–drain gap ($L = 5\,\mu m$), a second microstructure for which contact nucleated grains grow into the channel and then coalesce in the middle of the channel ($L = 20$–$25\,\mu m$), and a third microstructure with grain growth extending from the contact edges, but with a poorly ordered region in the middle of the channel ($L = 80\,\mu m$). We have investigated each of these three cases using SKPM and the results are discussed below.

Figure 1A shows typical drain current versus drain-to-source voltage (I_D vs. V_{DS}) characteristics for a device with a $5\,\mu m$ channel length and $800\,\mu m$ channel width. The nonideal behavior of this device (namely the curvature and compression of I_D at low V_{DS} in the linear region of device operation) is consistent with the presence of contact effects.[17,18] A mobility of $0.4\,cm^2\,V^{-1}\,s^{-1}$ is extracted from a plot of drain current versus gate-to-source voltage for the device biased in the saturation region (see Supporting Information). The mobility of these OTFTs exhibits a distinct channel length dependence with mobility decreasing as channel length increases (see Supporting Information). Such channel-length dependant mobility is the opposite of what would be expected for parasitic contact effects.[18] This apparent contradiction in

[*] Dr. J. G. Kushmerick, Dr. L. C. Teague,[+] Dr. B. H. Hamadani, Dr. O. D. Jurchescu, Dr. C. A. Richter, Dr. D. J. Gundlach
National Institute of Standards and Technology
Gaithersburg, MD 20899 (USA)
E-mail: james.kushmerick@nist.gov
S. Subramanian, Prof. J. E. Anthony
Department of Chemistry, University of Kentucky
Lexington, KY 40506 (USA)
Dr. O. D. Jurchescu, Prof. T. N. Jackson
Department of Electrical Engineering
The Pennsylvania State University
University Park, PA 16802 (USA)

[+] Present address: Savannah River National Laboratory, Aiken, SC 29808 (USA)

© 2008 WILEY-VCH Verlag GmbH & Co. KGaA, Weinheim

WILEY InterScience®
DISCOVER SOMETHING GREAT
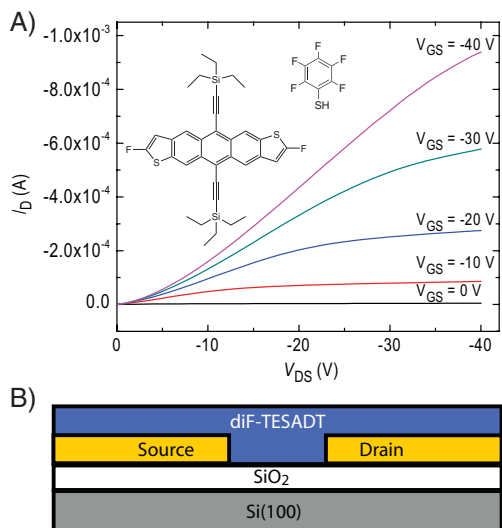
Figure 1. A) I_D versus V_{DS} characteristics for a diF-TESADT transistor with $L = 5\,\mu m$ and $W = 800\,\mu m$ at room temperature (inset) structure of diF-TESADT and PFBT. We note that diF-TESADT is a mixture of *syn-* and *anti-* isomers. Only the *anti-* isomer is shown here. B) Schematic of OTFT structure.

Figure 2. A) SKPM data of 5 μm OTFT device structure ($V_{DS} = -5$ V, $V_{GS} = -40$ V) the SKPM potential map (color) is overlaid on top of the corresponding 3-D topographic AFM image (see Supporting Information for separate images). The topographic and potential data were acquired simultaneously as described in the text. The horizontal dashed line in A) corresponds to the location of the topographic and potential line profiles shown in B), and the vertical dotted lines in B) indicate the location of the Au contact edges.

transport characteristics is one of the motivators for performing SKPM on these devices.

Figure 2A shows the SKPM image of the 5 μm channel OTFT from Figure 1A. From the topographic data we can clearly see that the diF-TESADT grain size is on the same order of magnitude as the channel length, and that single grains span the gap between the source and drain electrode (see Supporting Information). The potential profile (Fig. 2B) highlights that the main barrier to charge transport in this device is carrier injection into the organic semiconductor material from the source electrode. When the device is in the linear region ($V_{GS} = -40$ V $\gg V_{DS} = -5$ V) the primary voltage drop occurs at the source electrode–organic semiconductor contact, with only a gradual voltage drop across the organic semiconductor itself. Similar potential profiles reported for polymer-based TFTs were attributed to the Schottky barrier at the source/organic interface.[10] Unlike polymer systems, OTFTs fabricated from diF-TESADT are not homogenous and the interaction of the electrode-nucleated grains plays an important role in controlling the device properties as the channel length increases.

Figure 3A shows the SKPM image for a 20 μm channel OTFT. As the channel length increases the morphology of the active material within the channel begins to change. For devices on the order of $L = 20$–25 μm, a "ridge" of organic material in the center of the channel gives rise to a region of discontinuity in the active material, effectively a large grain boundary. The simplest explanation for the underlying cause of this "ridge" is that grains nucleated at the source and drain electrodes grow out into the channel and collide. The "ridge" is apparent in the topographic image but is further highlighted by the SKPM potential map since a pronounced voltage drop occurs at this boundary. It is clear that these grain boundaries
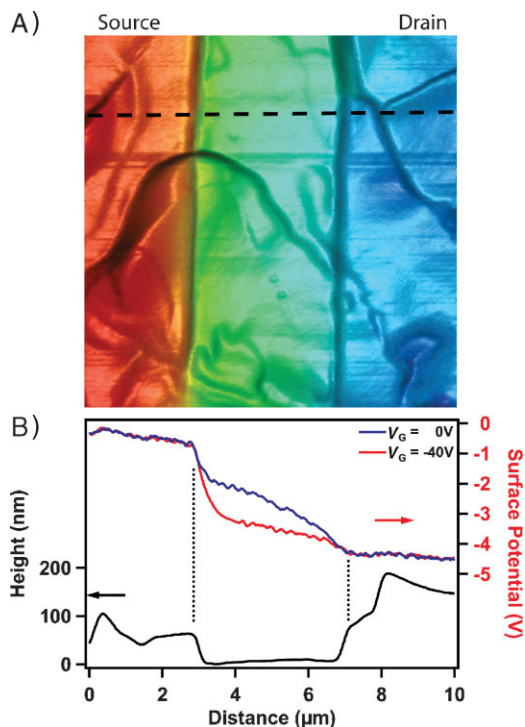
form a second barrier to charge transport in these devices. As the channel length is increased further the nature of the active material changes again.

Figure 4 shows the topographic and SKPM potential map for a portion of a 80 μm OTFT device. The topographic and SKPM channels are presented separately to highlight the transition in film morphology of the diF-TESADT layer. The left hand side of the image shows the diF-TESADT grains nucleated at and extending from the source electrode. The electrode itself is just off to the left of the image by ≈5 μm as determined from other scans of the area. Between 10 and 15 μm from the left edge of the image, the large diF-TESADT grains give way to a different film morphology. From previous studies we have determined that the diF-TESADT grains nucleated at the PFBT-treated contacts exhibit a two-dimensional π-stacking arrangement with the long axis of the ADT core near the plane of the surface (a situation optimal for charge transport via the π-system) while the orientation on silicon dioxide is significantly different and is made up of multiple crystal orientations.[15] The line profiles in Figure 4 demonstrate how the grains are nominally pinned at the source potential and that the voltage drops fairly linearly across the poorly nucleated, small grain diF-TESADT material in the middle of the channel. The full V_{DS} potential is not measured since the
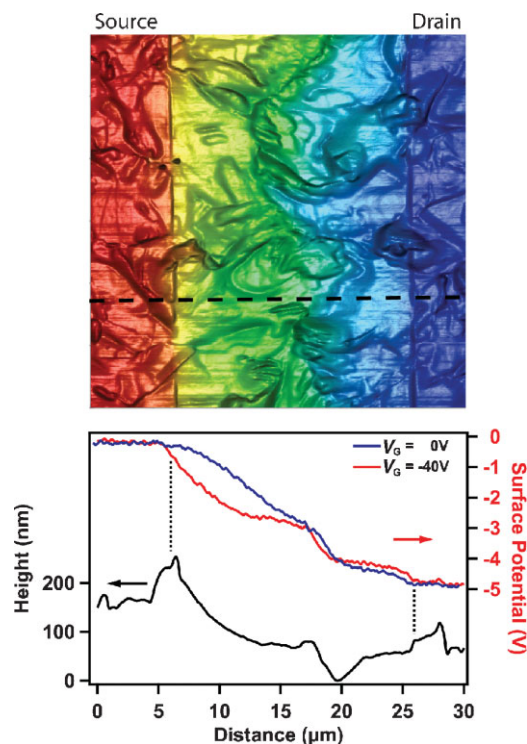
Figure 3. A) SKPM data of 20 μm OTFT device structure ($V_{DS} = -5$ V, $V_{GS} = -40$ V) the SKPM potential map (color) is overlaid on top of the corresponding 3-D topographic AFM image (see Supporting Information for separate images). The topographic and potential data were acquired simultaneously as described in the text. The horizontal dashed line in A) corresponds to the location of the topographic and potential line profiles shown in B), and the vertical dotted lines in B) indicate the location of the Au contact edges.

grains nucleated at the drain electrode are not in the field of view.

Collectively, this data gives us valuable insight into the role of channel length and film morphology on device mobility in these systems. The reason for decreasing mobility with increasing channel length for diF-TESADT OTFTs spun-cast on PFBT-functionalized electrodes is now quite clear. Charge transport in short channel devices (5 μm) is dominated by single diF-TESADT grains that span the channel. The main barrier to charge transport in these short channel devices is injection of carriers at the source electrode. Mid-length devices (20 μm) are characterized by the interaction of grain fronts extending from the two electrodes. In mid-length devices there are barriers associated with carrier injection as well as grain boundaries in the channel. Finally, the large channel devices are dominated by charge transport in the small-grain poorly nucleated diF-TESADT that grows on the silicon dioxide in the middle of the channel greater than ≈15 μm from the electrodes. The potential drop in these systems as measured by SKPM occurs almost exclusively over this region while the grains nucleated at the PFBT-treated electrodes are effectively pinned to the electrode potential.

In summary, our SKPM studies have provided a platform in which we were able to simultaneously probe the topography
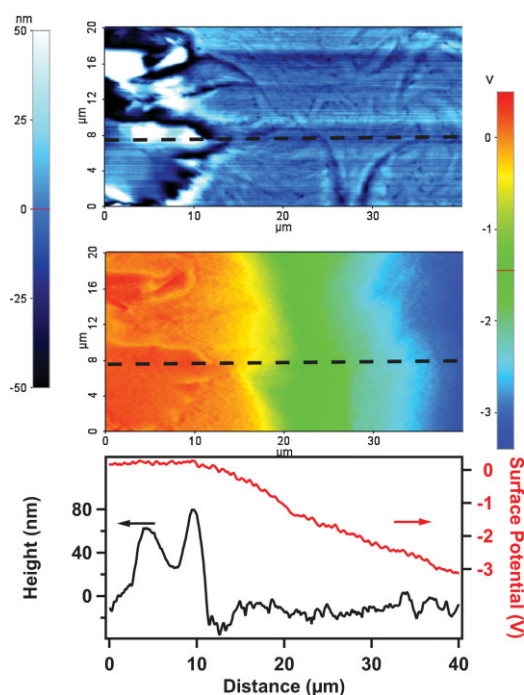

Figure 4. AFM topography (top) and SKPM data (middle) of a portion of a 80 μm OTFT device structure ($V_{DS} = -5$ V, $V_{GS} = -40$ V). The topographic and potential data were acquired simultaneously as described in the text. The left most portion of the images contain diF-TESADT grains extending from the source electrode. The horizontal dashed lines correspond to the location of the topographic and potential line profiles shown (bottom).

and the local potential drops within working OTFT devices. The data presented herein explicitly show a correlation between organic thin-film microstructure and potential drops within the working device. The nature and specific location of the potential drop varies with the device channel length for these systems. Short channel devices are dominated by the barriers at the organic/electrode interfaces. As the channel length increases, however, grain boundaries and regions of poorly nucleated material play a more important role in determining the mobility of the system. This work illustrates the importance of processing and metrology in the development of optimal low-cost, solution-processable organic electronic devices.

Experimental

The OTFTs studied here were fabricated in the following manner: diF-TESADT was prepared as described in the literature [19] and was spun cast at a rate of 1000 rpm from a 2 wt % solution in chlorobenzene (Ar environment) onto ultraviolet ozone cleaned, thermally oxidized heavily doped Si(100) substrates with Ti/Au (≈5 and ≈40 nm, respectively) source and drain contacts modified with PFBT. Simultaneous topographic and surface potential data for the device structures was obtained under ambient conditions using the Scanning Kelvin probe mode of a XE100 atomic force microscope (Park Systems, Santa Clara, CA, USA [20]). Briefly, the AFM is operated in amplitude modulation mode with Pt coated Si cantilevers, with a

nominal resonant frequency of 150–300 kHz. An AC bias (17 kHz, 3 V RMS) is applied to the tip and a lock-in amplifier is used to measure the resulting electrostatic force due to the surface potential difference between the AFM tip and device surface. A feedback loop is used to null this electrostatic force by applying a DC bias to the tip and it is this applied bias that provides a direct measurement of the surface potential. Drain–source voltages (V_{DS}) and gate voltages (V_{GS}) were applied to the devices (mounted in a ceramic DIP) with a semiconductor parameter analyzer. The source–drain current did not fluctuate appreciably over the timescale of the SKPM measurements (≈ 5 min per scan).

[1] G. Horowitz, *Adv. Mater.* **1998**, *10*, 365.

[2] H. Sirringhaus, *Adv. Mater.* **2005**, *17*, 2411.

[3] C. D. Dimitrakopoulos, P. R. L. Malenfant, *Adv. Mater.* **2002**, *14*, 99.

[4] K. Seshadri, C. D. Frisbie, *Appl. Phys. Lett.* **2000**, *78*, 993.

[5] T. W. Kelley, C. D. Frisbie, *J. Phys. Chem. B* **2001**, *105*, 4538.

[6] A. B. Chwang, C. D. Frisbie, *J. Appl. Phys.* **2001**, *90*, 1342.

[7] K. P. Puntambekar, P. V. Pesavento, C. D. Frisbie, *Appl. Phys. Lett.* **2003**, *83*, 5539.

[8] J. A. Nichols, D. J. Gundlach, T. N. Jackson, *Appl. Phys. Lett.* **2003**, *83*, 2366.

[9] L. Bürgi, H. Sirringhaus, R. H. Friend, *Appl. Phys. Lett.* **2002**, *80*, 2913.

[10] L. Bürgi, T. J. Richards, R. H. Friend, H. Sirringhaus, *J. Appl. Phys.* **2003**, *94*, 6129.

[11] L. Chen, R. Ludeke, X. Cui, A. G. Schrott, C. R. Kagan, L. E. Brus, *J. Phys. Chem. B* **2005**, *109*, 1834.

[12] Y. Luo, F. Gustavo, J.-Y. Henry, F. Mathevet, F. Lefloch, M. Sanquer, P. Rannou, B. Grevin, *Adv. Mater.* **2007**, *19*, 2267.

[13] K. P. Puntambekar, J. Dong, G. Haugstad, C. D. Frisbie, *Adv. Funct. Mater.* **2006**, *16*, 879.

[14] S. K. Park, C. C. Kuo, J. E. Anthony, T. N. Jackson, *IEDM Tech. Digest* **2005**, *113*.

[15] D. J. Gundlach, J. E. Royer, S. K. Park, S. Subramanian, O. D. Jurchescu, B. H. Hamadani, A. J. Moad, R. J. Kline, L. C. Teague, O. Kirillov, C. A. Richter, J. G. Kushmerick, L. J. Richter, S. R. Parkin, T. N. Jackson, J. E. Anthony, *Nat. Mater.* **2008**, *7*, 216.

[16] O. D. Jurchescu, B. H. Hamadani, H. D. Xiong, S. K. Park, S. Subramanian, N. M. Zimmerman, J. E. Anthony, T. N. Jackson, D. J. Gundlach, *Appl. Phys. Lett.* **2008**, *92*, 132103.

[17] D. J. Gundlach, L. Jia, T. N. Jackson, *IEEE Electron Device Lett.* **2001**, *22*, 571.

[18] D. J. Gundlach, L. Zhou, J. A. Nichols, T. N. Jackson, P. V. Necliudov, M. S. Shur, *J. Appl. Phys.* **2006**, *100*, 024509.

[19] S. Subramanian, S. K. Park, S. R. Parkin, V. Podzorov, T. N. Jackson, J. E. Anthony, *J. Am. Chem. Soc.* **2008**, *130*, 2706.

[20] Certain commercial equipment, instruments, or materials are identified in this paper to foster understanding. Such identification does not imply recommendation or endorsement by the National Institute of Standards and Technology, nor does it imply that the materials or equipment identified are necessarily the best available for this purpose.